A RAY TRACING TECHNIQUE FOR COVERAGE PREDICTIONS IN MICRO CELLULAR ENVIRONMENTS

M. E. C. Rodrigues[1], L. A. R. Ramirez[2], L. A. R. Silva Mello[2] and F. J. V. Hasselmann[2]

[1]WiNGS Telecom
Rio de Janeiro 20040-020, Brazil
[2]CETUC - Center for Telecommunications Studies
Catholic University of Rio de Janeiro
RJ 22453-900, Brazil

ABSTRACT

This work presents a 3D vector formulation for calculation of the field scattered by finite conductivity wedges, developed as an extension of the Uniform Theory of Diffraction (UTD) version for perfect conductors, representative of obstacles usually encountered in both indoor and outdoor environments served by cellular communication systems. Its main contribution consists, aside from the 3D vector treatment for the problem at hand, of the definition of diffraction coefficient parameters associated to virtual reflections on the wedge shadowed face. The singular behavior of diffraction coefficients thus obtained, along regions coincident with (real and virtual) geometrical shadow boundaries, as well as the resulting reciprocity of the formulation in terms of the arbitrary choice of the wedge illuminated face, indicate its adequacy. The formulation is next applied to the calculation of propagation path losses and delay profiles for typical building layouts. Implementation aspects of launching, tracing and capturing relevant optical rays as well as applying the Quadtree method for spatial (scenario) discrimination are also discussed.

Key words: cellular communications; ray tracing; diffraction; UTD

1. INTRODUCTION

Modern cellular communication systems planing and design have addressed both micro and picocell operation, for which former empirical methods of coverage assessment can no longer yield the required accuracy. Among reliable options, one depicts the so-called ray tracing technique, whereby the electromagnetic field is tracked along trajectories orthogonal to wavefronts from source to observation point, directly and via the scattering route. The first part of this work focuses in the accompanying establishment of a 3D vector formulation for the field scattered by typical obstacles which might be employed together with appropriate ray tracing techniques.

 ISSN 1516-7399

EM field tracking along reflected and diffracted rays is usually accomplished by making use of UTD formulations, developed from appropriate asymptotic approximations for the canonical problem of scattering by perfectly conducting (PEC) wedges in the high-frequency regime [1]. In a typical indoor or outdoor cellular communications environment, it is often adequate to represent large obstacles encountered (e.g. corridor walls and buildings) by multi-faceted plane assemblages, therefore allowing for the development of unified computer codes without incurring in frequent and time-consuming calculations of diverse geometrical features. In view of this, the need arises for an extension of UTD that might handle, in a 3D vector fashion, the scattering properties of plane though finite-conductivity wedges and, at the same time, be so formulated as to permit its encompassing by engineering oriented software, which does not seem to be so simple with recent applications of the so-called Maliuzhinets method [2, 3]. As detailed in [4], its application to impedance wedges of arbitrary angles and/or under skew incidence (as inherent to 3-D vector formulations), requires the approximate solution of coupled difference equations. On the other hand, its implementation for the right-angle wedge under normal (to the edge) plane wave incidence in Aïdi and Lavergnat´s recent study [5] reveals no significant improvement over their own modification of the more common heuristic approach in (less cumbersome) Leubbers´s formulation [6] for most aspects of observation, rendering the latter better suited for that application. In time, their modification of Leubber´s (inappropriate) heuristic diffraction coefficient was introduced to satisfy the necessary invariance of the diffraction coefficient relatively to the arbitrary choice of the reference wedge face as well as the requirement of null diffraction coefficient for grazing incidence.

A physically transparent and geometrically interpretable formulation may, nonetheless, be heuristically introduced via the substitution of soft and hard (±1) reflection coefficients in the UTD version for PEC wedges by appropriate Fresnel coefficients, as attempted in [6] and employed by many [e.g. 7]. An important remark, referring to the definition of incidence angles for shadowed wedge faces as they arise in reflection and, consequently, diffraction coefficients, is in order. These virtual reflections are herein treated in a coherent way, following the treatment for face curvatures in perfectly conducting wedges outlined in [8] and leading to shadow boundaries along the same regions as expected by inspection of (thus obtained) diffraction coefficients singularities. It is also ascertained the formulation reciprocity as per the definition of the wedge “0” and “n” (lit and shadowed) faces and inherent angular parameters in the plane orthogonal to the edge, an additional indicative of its adequacy.

A major undertaking towards its implementation for complex scenarios consists of developing suitable acceleration routines to account for up to thousands of optical (ray) paths relevant to usual coverage calculations. In this regard, also important are the choice of ray launching and capturing strategies as well as the proper perception of trade-offs between conventional image and shooting & bouncing methods to account for relevant reflection and/or diffraction specular (obstacle) points and corresponding scattering mechanisms. The basic features of these (ray) techniques and methods of field calculation, along with those pertaining to the Quadtree space discrimination method for purposes of optimizing scenario descriptions, are reviewed in what follows. A combined implementation of the above for typical idealized environments yielded the illustrative results for propagation path losses and power delay profiles (PDP).

2. UTD FOR FINITE CONDUCTIVITY OBSTACLES

The EM field scattered by obstacles is composed, according to UTD, of reflected and diffracted field contributions. The field reflected at the interface between free space and a

 ISSN 1516-7399

medium of depth much larger than the wavelength and (effective) electrical relative permittivity $\varepsilon_{efr} = [\varepsilon - j(\sigma/w)]/\varepsilon_o$, where σ and w denote, respectively, the conductivity of the material and the working frequency, is expressed, along its components perpendicular (soft) and parallel (hard) to the incidence plane containing incident ray and surface normal directions, and for the parameters defined in Figure 1, by

$$\vec{E}^r(O) = \left[E^r_{\alpha_2}\hat{\alpha}_2 + E^r_{\beta_2}\hat{\beta}_2\right] A^r \; e^{-jkd_2} \tag{1}$$

where

$$\begin{pmatrix} E^r_{\alpha_2} \\ E^r_{\beta_2} \end{pmatrix} = \begin{pmatrix} \Gamma_s & 0 \\ 0 & \Gamma_h \end{pmatrix} \begin{pmatrix} \vec{E}^i(R).\hat{\alpha}_1 \\ \vec{E}^i(R).\hat{\beta}_1 \end{pmatrix} \tag{1a}$$

$$\hat{\alpha}_{1,2} = \frac{\hat{s}_{1,2} x\, \hat{n}}{\left|\hat{s}_{1,2} x\, \hat{n}\right|} \qquad \hat{\beta}_{1,2} = \hat{s}_{1,2} x\, \hat{\alpha}_{1,2} \tag{1b}$$

$$\hat{s}_2 = \frac{\vec{s}_2}{\left|\vec{s}_2\right|}, \; \vec{s}_2 = \hat{s}_1 - 2(\hat{n}.\hat{s}_1)\hat{n} \tag{1c}$$

$$A^r = \sqrt{\frac{\rho^r_1 \rho^r_2}{\left(\rho^r_1 + d_2\right)\left(\rho^r_2 + d_2\right)}} \tag{1d}$$

with ρ^r denoting the reflected wave principal radii of curvature (equal to those of the incident wave for reflections at plane interfaces) at the reflection point (R), d_2 the distance between reflection and observation points, and, for an incidence angle θ_i, the Fresnel reflection coefficients

$$\Gamma_s(\theta_i) = \frac{\cos(\theta_i) - \sqrt{\varepsilon_{efr} - sen^2(\theta_i)}}{\cos(\theta_i) + \sqrt{\varepsilon_{efr} - sen^2(\theta_i)}}$$

$$\Gamma_h(\theta_i) = \frac{\varepsilon_{efr}\cos(\theta_i) - \sqrt{\varepsilon_{efr} - sen^2(\theta_i)}}{\varepsilon_{efr}\cos(\theta_i) + \sqrt{\varepsilon_{efr} - sen^2(\theta_i)}} \tag{2}$$

For indoor communications, one also takes into account reflection and transmission mechanisms at/through material walls; corresponding Fresnel coefficients and (transmitted) field tracking expressions, as well as those for reflection and/or refraction at arbitrarily curved interfaces, are listed in [9].

 ISSN 1516-7399

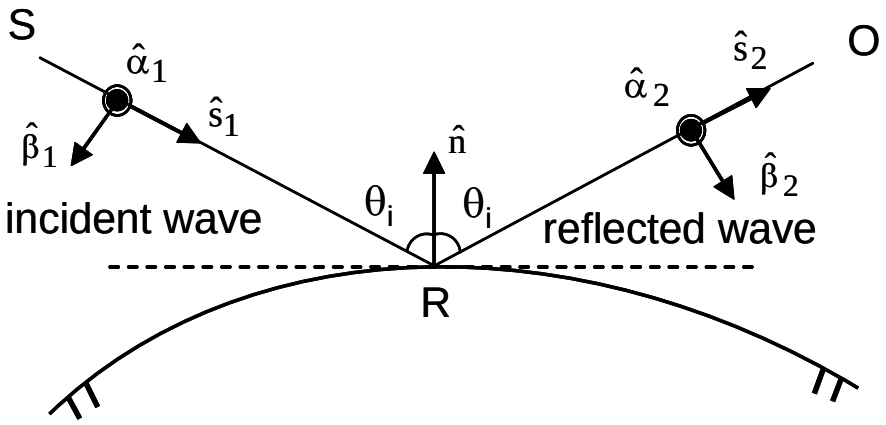

Figure 1 Ray-fixed coordinate systems for reflection (view from incidence plane)

Figure 2 illustrates the relevant parameters pertaining to the diffraction by a wedge consisting of plane walls and a straight edge; a view from the plane normal to the diffraction edge is shown in Figure 3. Diffracted and incident fields, expressed along their components parallel (soft) and perpendicular (hard) to edge-fixed planes of diffraction/incidence (containing diffracted/incident ray directions and unit vector ê tangent to the edge), relate to each other via

$$\vec{E}^{\,d}(O) = \left[E_\beta^d \hat{\beta} + E_\phi^d \hat{\phi}\right] A^d \; e^{-jkd_2} \tag{3}$$

with

$$\begin{pmatrix} E_\beta^d \\ E_\phi^d \end{pmatrix} = \begin{pmatrix} -D_s & 0 \\ 0 & -D_h \end{pmatrix} \begin{pmatrix} \vec{E}^{\,i}(Q).\hat{\beta}' \\ \vec{E}^{\,i}(Q).\hat{\phi}' \end{pmatrix} \tag{3a}$$

$$\hat{\phi}^{(')} = \frac{\hat{e}\, x\, \hat{s}^{(')}}{\left|\hat{e}\, x\, \hat{s}^{(')}\right|} \qquad \hat{\beta}^{(')} = \hat{\phi}^{(')}\, x\, \hat{s}^{(')} \tag{3b}$$

$$\hat{s} = \frac{\vec{s}}{|\vec{s}|}, \quad \vec{s} = (\hat{s}'.\hat{e})\hat{e} + \left|\hat{s}'\, x\, \hat{e}\right|\left[(\cos\phi)\hat{f} + (sen\phi)\hat{n}_0\right] \tag{3c}$$

$$\cos\phi^{(')} = \frac{\vec{s}^{\,(')}_{proj.}.\hat{f}}{\left|\vec{s}^{\,(')}_{proj.}\right|} \quad , \quad \vec{s}^{\,(')}_{proj.} = \hat{s}^{(')} - \left(\hat{s}^{(')}.\hat{e}\right)\hat{e} \tag{3d}$$

$$A^d = \sqrt{\frac{\rho_1^d}{\sigma(\rho_1^d + \sigma)}} \tag{3e}$$

where ρ^d denotes the diffracted ray tube caustic distance (equaling, for plane wedges, the radius of curvature of the incident wave in the edge-fixed incident plane [9]), σ the distance

 ISSN 1516-7399

between diffraction and observation points and, for a wedge internal angle $\psi = (2–n)\pi$, the diffraction coefficients

$$D_{s,h}(L,\phi,\phi',\delta,n) = G_{o\,s,h}\left(D_1 + \Gamma_{o_{s,h}} D_2\right) + G_{n_{s,h}}\left(D_3 + \Gamma_{n_{s,h}} D_4\right) \tag{4}$$

with grazing incidence factors

$$G_{0(n)_{s,h}} = \begin{cases} \dfrac{1}{1+\Gamma_{0(n)_{s,h}}} \quad , \quad \phi' = 0(\mathrm{n}\pi), \quad \left|1+\Gamma_{0(\mathrm{n})}\right| > 0 \\ 1/2 \quad , \quad \phi' = \mathrm{n}\pi(0) \\ 1 \quad , \quad \text{otherwise} \end{cases} \tag{4a}$$

and

$$\begin{aligned} D_1 &= \frac{-e^{-j\pi/4}}{2n\sqrt{2k\pi}\,sen\delta}\cot\left[\frac{\pi-(\phi-\phi')}{2n}\right]F\left[kL^i a^-(\phi-\phi')\right] \\ D_2 &= \frac{-e^{-j\pi/4}}{2n\sqrt{2k\pi}\,sen\delta}\cot\left[\frac{\pi-(\phi+\phi')}{2n}\right]F\left[kL^{ro} a^-(\phi+\phi')\right] \\ D_3 &= \frac{-e^{-j\pi/4}}{2n\sqrt{2k\pi}\,sen\delta}\cot\left[\frac{\pi+(\phi-\phi')}{2n}\right]F\left[kL^i a^+(\phi-\phi')\right] \\ D_4 &= \frac{-e^{-j\pi/4}}{2n\sqrt{2k\pi}\,sen\delta}\cot\left[\frac{\pi+(\phi+\phi')}{2n}\right]F\left[kL^{rn} a^+(\phi+\phi')\right] \end{aligned} \tag{4b}$$

In the above expressions, one defines, with $N^{\pm}$ representing integers that most closely satisfy equations $2\pi N^{+(-)} - \beta^{\pm} = +(-)\pi$ and $\beta^{\pm} = \phi \pm \phi'$, angular separation measures between observation point and an incidence or reflection shadow boundary

$$a^{\pm}(\beta) = 2\cos^2\left(\frac{2n\pi N^{\pm} - \beta}{2}\right), \tag{4c}$$

the Fresnel transition function

$$F(x) = 2j\sqrt{x}\,e^{jx}\int_{\sqrt{x}}^{\infty}\exp\left(-j\tau^2\right)d\tau \tag{4d}$$

and distance parameters associated to “0” and “n” faces

 ISSN 1516-7399

$$L^{i,r_{o,n}} = \frac{\sigma\left(\rho_e^{i,r_{o,n}} + \sigma\right)\rho_1^{i,r_{o,n}}\rho_2^{i,r_{o,n}}\left(1-(\hat{s}'.\hat{e})^2\right)}{\rho_e^{i,r_{o,n}}\left(\rho_1^{i,r_{o,n}} + \sigma\right)\left(\rho_2^{i,r_{o,n}} + \sigma\right)} \tag{4e}$$

where $\rho^{i,r}_{1,2}$ and $\rho^{i,r}_{e}$ denote respectively, for for both wedge faces, the principal radii of curvature of incident/reflected waves and those in edge-fixed incidence/reflection planes, as calculated at the diffraction point and with σ along incidence/reflection shadow boundaries. A detailed treatment of simple and multiple diffraction, as well as the occurrence of alternate reflections and diffraction, is presented in [9], where approximate expressions for the Fresnel function in (4d), adequate for different ranges of its argument with respect to relative positions of observation point and transition regions around shadow boundaries, are also listed and have their accuracy ascertained.

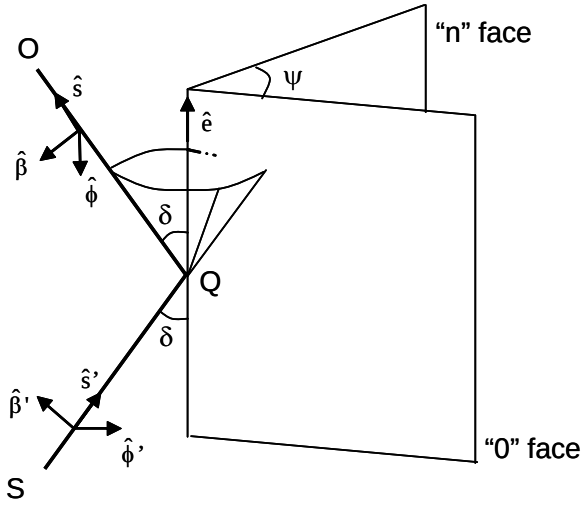

Figure 2 Straight wedge diffraction cone and ray-fixed coordinate systems

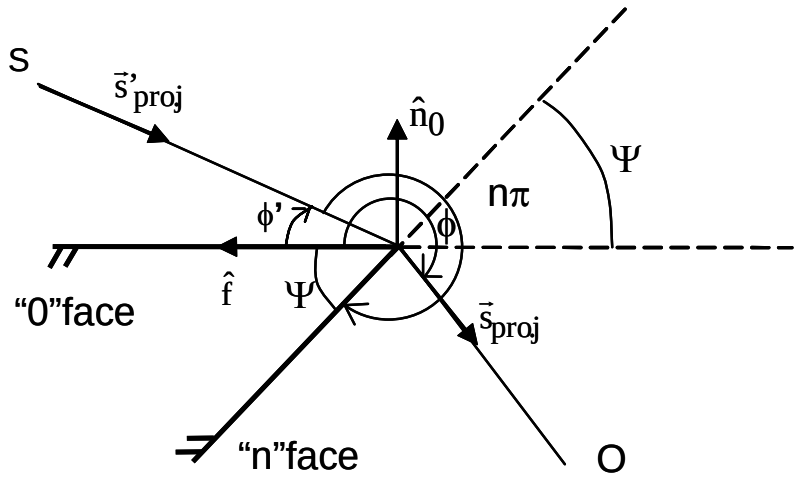

Figure 3 View from plane normal to the edge

Due to lack of an exact solution for the problem at hand, that might be asymptotically approximated in a convenient way, Fresnel reflection coefficients, inserted in (4) as a replacement for their counterparts in the UTD formulation for scattering by PEC wedges [1], are those in (2) for outdoor communications albeit special attention is now required when defining (virtual) incidence angles for shadowed ("0" or "n") faces. A key factor is the condition $\cos(\theta i_{0,n}) \geq 0$, i.e. $0 \leq \theta i_{0,n} \leq \pi/2$, now imposing that the unit vector normal to the shadowed face must have its conventional orientation inverted, as illustrated in Figure 4.

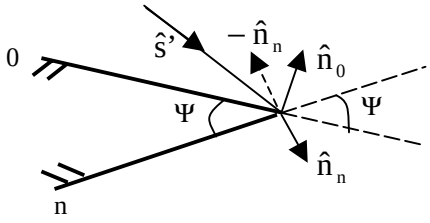

$$\text{for } \Gamma_{0_{s,h}} : \theta_i = \theta_{i_0} = \arccos(-\hat{n}_0.\hat{s}')$$
$$\text{for } \Gamma_{n_{s,h}} : \theta_i = \theta_{i_n} = \arccos(\hat{n}_n.\hat{s}')$$

(a) "0" face illuminated

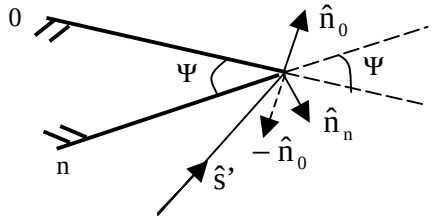

$$\text{for } \Gamma_{0_{s,h}} : \theta_i = \theta_{i_0} = \arccos(\hat{n}_0.\hat{s}')$$
$$\text{for } \Gamma_{n_{s,h}} : \theta_i = \theta_{i_n} = \arccos(-\hat{n}_n.\hat{s}')$$

(b) "n" face illuminated

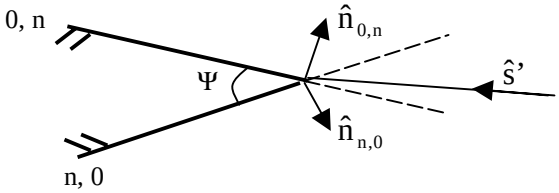

$$\text{for } \Gamma_{0_{s,h}} : \theta_i = \theta_{i_0} = \arccos(-\hat{n}_0.\hat{s}')$$
$$\text{for } \Gamma_{n_{s,h}} : \theta_i = \theta_{i_n} = \arccos(-\hat{n}_n.\hat{s}')$$

(c) both faces illuminated

Figure 4 Definition of incidence angles and normal unit vectors

This definition also implies (real or virtual) geometrical incidence/reflection shadow boundaries in accordance with their mathematical definitions, which correspond to the centers of transition regions where a factor cot(x) in (4b) tends to infinity – being remedied by a finitely limited product by accompanying Fresnel functions – as depicted from cross

 ISSN 1516-7399

examining Table 1 and the view from a plane normal to the edge in Figure 5. Numerical results also evidenced [6] that the solution above proposed is symmetrical with respect to the definition of the lit ("0") face, with values of diffraction coefficients Ds,h maintained in spite of altered $\beta\pm$ values due to interchanging ϕ and ϕ', in (4), for a given pair of incident/reflected rays. This attained reciprocity feature reinforces the overall adequacy of the formulation thus obtained.

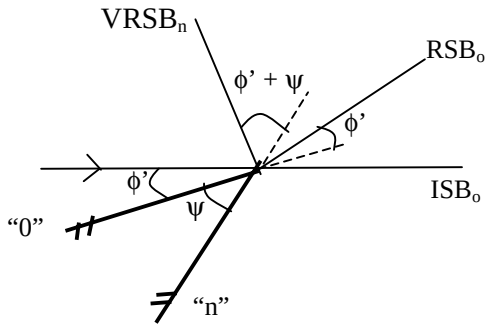

$ISB_o : \phi = \phi' + \pi$
$RSB_o : \phi = \pi - \phi'$,
$VRSB_n : \phi = (2n - 1)\,\pi - \phi'$

(a) "0" face illuminated

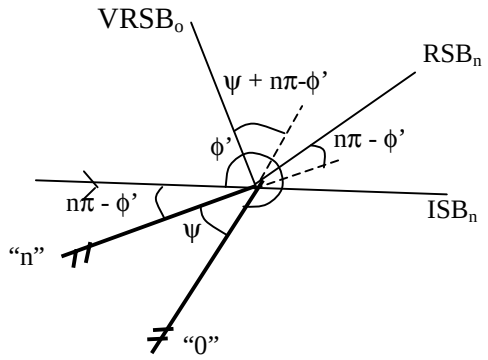

$ISB_n : \phi = \phi' - \pi$
$RSB_n : \phi = (2n- 1)\pi - \phi'$
$VRSB_o : \phi = \pi - \phi'$

(b) "n" face illuminated

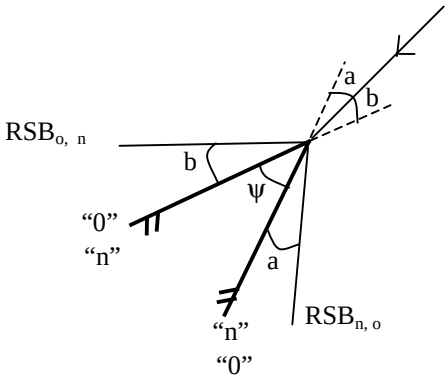

$RSB_o : \phi = \pi - \phi'$
$RSB_n : \phi = (2n - 1)\,\pi - \phi'$

(c) both faces illuminated

Figure 5 Description of real and virtual shadow boundaries

For highly tapered low edge illumination levels, one must also consider the second order effect known as slope diffraction, whereby soft and hard field components, proportional to derivatives of 1st order diffraction coefficients and those of incident field components in the plane normal to the edge, are added to the main diffracted field. Full slope-field analytical expressions are derived in [9] for the situations where just one or both wedge faces are illuminated, being overlooked herein due to space considerations.

 ISSN 1516-7399

TABLE 1 Location of incidence and reflection shadow boundaries for "0"and "n" faces

cotangent function for each shadow boundary	cotangent function is singular at (shadow boundary location)	value of N at shadow boundary
$\cot\left(\frac{\pi+(\phi-\phi')}{2n}\right)$	$\phi = \phi' - \pi$ (argument of *cot(x)* is null) ISB_n boundary	$N^+ = 0$
$\cot\left(\frac{\pi-(\phi-\phi')}{2n}\right)$	$\phi = \phi' + \pi$ (argument of *cot(x)* is null) ISB_0 boundary	$N^- = 0$
$\cot\left(\frac{\pi+(\phi+\phi')}{2n}\right)$	$\phi = (2n - 1)\,\pi - \phi'$ (argument of *cot(x)* is π) (real ou virtual) RSB_n boundary	$N^+ = 1$
$\cot\left(\frac{\pi-(\phi+\phi')}{2n}\right)$	$\phi = \pi - \phi'$ (argument of *cot(x)* is null) (real ou virtual) RSB_n boundary	$N^- = 0$

3. TECHNIQUES AND REPRESENTATIONS

A. Representation of Solids

A method of representation of solids for use in conjunction with ray tracing techniques has been implemented [10] by making use of vector (dxf) files properly modified to include estimated electrical properties (permittivity and conductivity) of materials as well as changes in forms for greater compatibility with the graphical routines of public library OpenGL[11].

B. Ray Tracing

Following usual ray tracing techniques (Figure 6), rays may be homogeneously emitted from a unit sphere centered at the transmitter phase center location, in what is known as the ray launching method, and being therefore able to cover all observation regions evenly. Throughout its implementation, all possible (ray) paths from transmitter to receiver are traced and corresponding fields (line-of-sight transmission, ground reflection, multiple specular reflections on walls, diffractions by building corners and over rooftops) [10]. Conversely, one may employ the method of images (Figure 7), whereby new (virtual) sources are created at image (with respect of walls) locations of existing (actual or real) sources. In this way, each contributing (to field calculation) ray path from transmitter to receiver is determined. In complex scenarios with a large number of solids, however, implementation of this scheme may become intractable with the increase in the number of image.

 ISSN 1516-7399

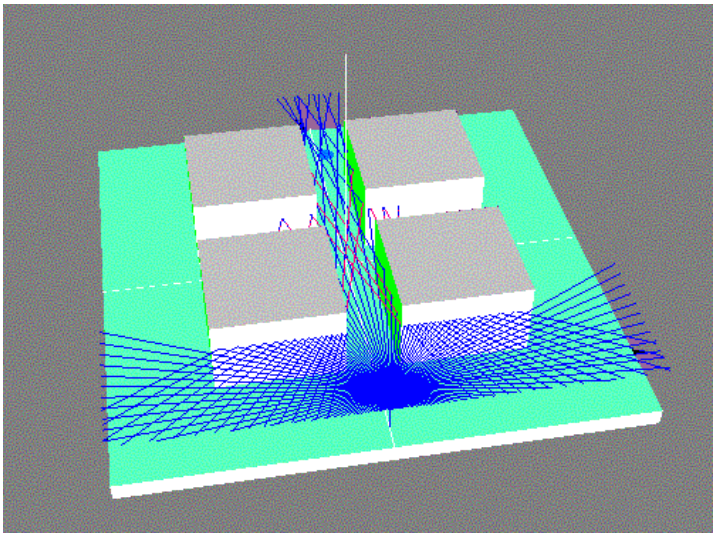

Figure 6 Visualization of ray tracing mechanisms using the ray launching method for up to 4 reflections in the Tx-Rx plan

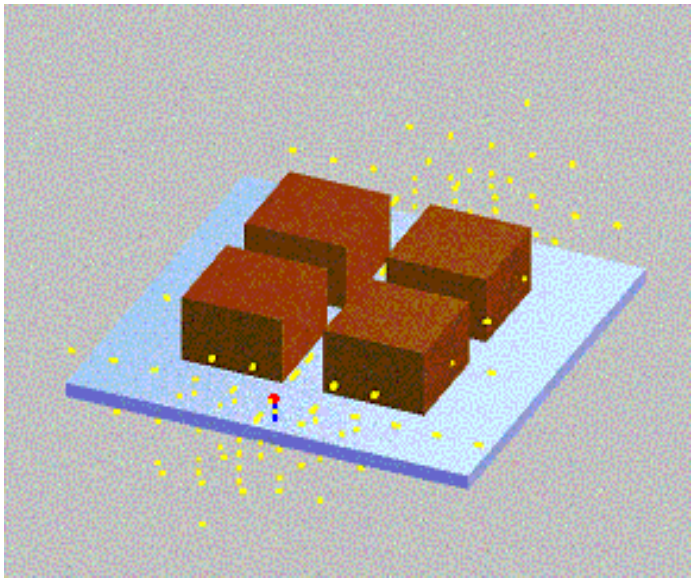

Figure 7 Example of image method implementation with primary source location in red and those of following images in yellow

As reviewed in Section 2, an extension of the Uniform Theory of Diffraction has been formulated so as to accommodate the diffraction by obstacles of finite conductivity, such as buildings in a cellular environment. In this way, proper high-frequency asymptotic are able to deal with relevant scattering mechanisms that occur, e.g. in a block corner, in a uniform fashion about shadow boundaries and intervening transition regions as illustrated in Figure 8. The resulting (3D vector) formulations were implemented in [10] and comprise the foundation of field calculations presented herein in conjunction with ray tracing schemes.

 ISSN 1516-7399

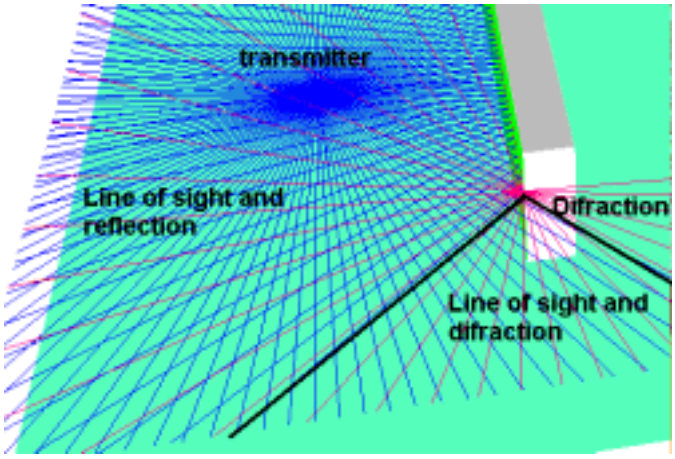

Figure 8 Field coverage regions around building corners

Another critical problem, actually faced by both techniques, refers to solid forms, since one is limited to multi-faceted plane assemblages in order to obtain source images and avoid introducing too many degrees of freedom in the directions of diffracted rays [10]. Implementations of ray tracers that combine both methods above may be found in [12, 13, 14, 15]. Usage of the image method was hereby preferred with a view towards future implementations considering complex scenarios eventually conformed by solids with curved faces as well.

C. Ray Launching and Capturing

Three ray launching schemes to obtain homogenized emissions from a transmitter centered sphere are illustrated in Figure 9. In the scheme (a) of spherical coordinates, the partition of azimuth and elevation angles in equal increments fails because, in the polar regions, the sphere has clusters of dense vertices while those in the equator are spaced. In scheme (b), the increment in azimuth angle varies with the sine of elevation angles, also rendering irregular partitions. In scheme (c), implemented herein after [10], the vertex of the geodesic sphere foresees a uniform distribution for the spacing of vertices, as a result of the division in the faces of regular icosahedrons [17].

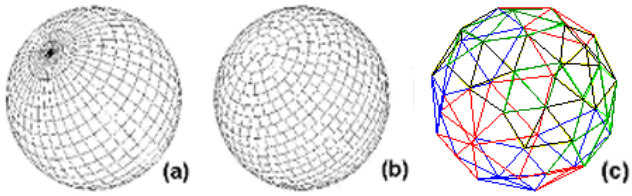

Figure 9 Schemes for homogenized emission of rays: (a) system of spherical coordinates; (b) scheme proposed in [16]; (c) scheme of geodesic spheres proposed in [17] and implemented in [10]

As for the reception sphere, it is centered at the receptor and sized according to the angular separation of the incoming rays for proper collection of those contributing to the overall electric field, as illustrated in Figure 10. The minimum radius for a reception sphere to ensure capturing at least one ray per wave front corresponds to $1/\sqrt{3}$ of the distance between adjacent rays [18].

 ISSN 1516-7399

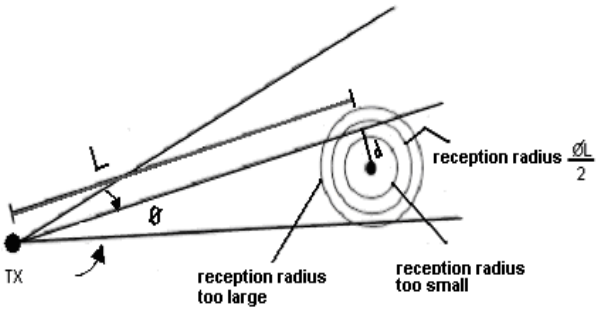

Figure 10 Unfolded ray path (L) and reception area defined by circle of radius ϕL/2 [19]

D. Scenario Discrimination

The basic principle of the Quadtree spatial discrimination technique is to describe objects via a hierarchic structure of data based on a recursive decomposition of the bi-dimensional space, as governed by the very properties of the input data. As an example, the map of the city may be covered by a rectangle (representing the knot root of the tree), which is divided recursively in quadrants of decreasing size until their number satisfies a prescribed inferior limit, resulting in the hierarchic (spatial) structure of the tree as illustrated in Figure 11. This process permits to reduce the object number contained in the knot, along with the subdivision level, aiming at the minimization of the number of ray intersections with the solid to be searched for and, consequently, the amount of memory necessary to store the tree. Other methods of spatial discrimination have been studied, such as the 3D generalization of the Quadtree method, known as Octatree, and the Binary Spatial Partition (BSP) method, ideal for bigger and more complex environments.

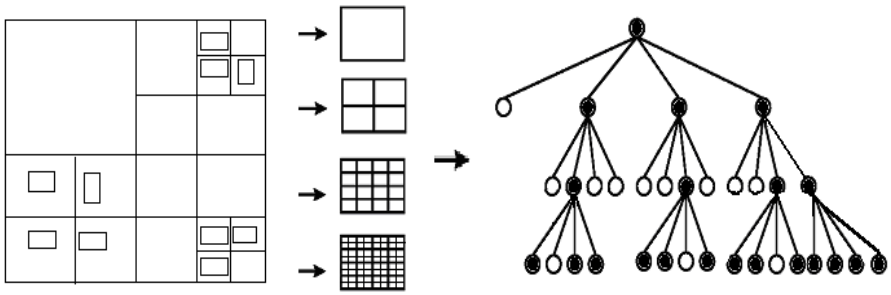

Figure 11 Example of a Quadtree subdivision of a city map

For the present implementation, the choice resided in the Quadtree technique, considered as an algorithm base for the Octree upgrade, in view of the fact that the environments considered herein comprise only antenna heights inferior to those of the buildings in the scenario [10].

E. Path Loss and Power Delay Profile

The propagation path loss parameter (L), defined as the ratio between transmitted (Pt) and received (Pr) power levels, is commonly used to characterize the local average signal in a mobile channel, with its accurate prediction rendering an estimation of the radiowave coverage area. Also important in the characterization of mobile channels is the plot of different (for a selected transmitter – receiver pair) ray-path arrival times, relative to the line-of-sight path arrival time, versus corresponding received power levels, the so-called power

 ISSN 1516-7399

delay profile (PDP); its accurate assessment is fundamental for establishing inter-symbolic interferences and, thus, bit error rates in wideband digital systems.

Once identified all relevant ray-paths between transmitter and receiver antennas in a given environment, one proceeds with the optimization scheme of spatial representations and apply UTD for corresponding EM field tracking, yielding the desired path loss and the power delay profile calculations as developed in [10] and exemplified in the following selected results.

4. SOME RESULTS AND DISCUSSION

Figures 12 and 14 depict the basic environment cells used for the simulation tests of the techniques cited above and appraisal of corresponding results. The scenario comprehends an area of roughly 200m x 200m with buildings represented by solids of 30m (approximately 8 floors) maximum heights. Locations of transmitter and receiver, together with characteristic parameters, are specified, in the developed computer code, via a typical user friendly window interface [10]. In what follows, both transmitter and receiver are modeled by isotropic antennas and, for the building walls, a relative effective permittivity $\varepsilon r = 15 - j90 / f[MHz]$ is used. Remaining relevant parameters, such as frequency, field polarization (horizontal / vertical), transmitted power and the number of reflections to be considered are also established via the user input interface, as illustrated for the scenarios at hand in Figures 12 and 14 for Tx-Rx in line-of-sight (LOS) and in Fig. 16 for a shadowed receiver. Also, up to two corner diffractions have been implemented for considered ray trajectories in the study cases presented, as illustrated in figures 12, 14 and 16, where purely reflected rays are traced in blue color and the evolution of diffracted rays is shown in red.

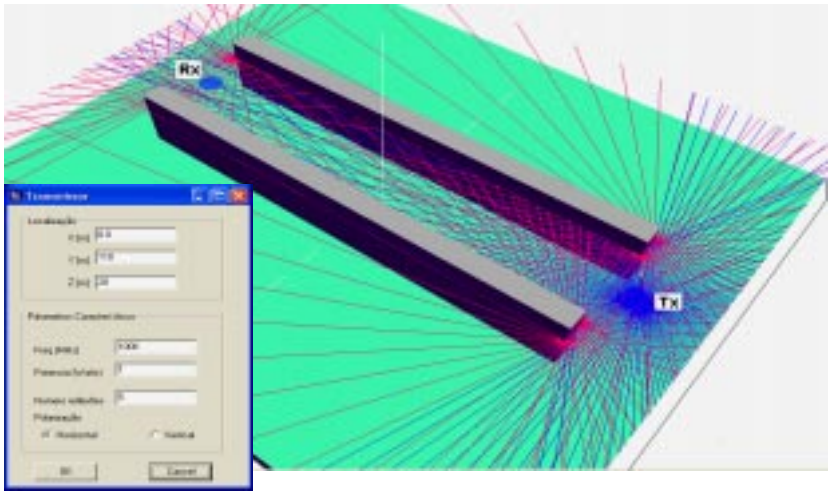

Figure 12 LOS case study: Pt =1W, f =1Ghz, horizontal polarization, transmitter height = 18 m, receptor height = 2 m, 5 reflections and up to 2 diffractions considered

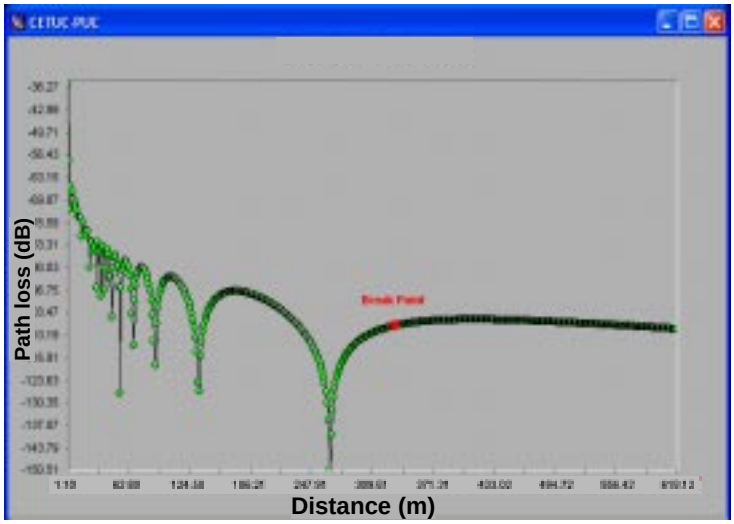

Figure 13 Predicted path loss along LOS corridor for the configuration in Figure 12

In Figures 13 and 15 one can identify two regions were the received signal show different behaviors. In the first region the signal undergoes strong fluctuations due to the interference between the direct and reflected rays, including those that have undergone (up to two) diffractions amid reflections; purely diffracted fields, whenever corresponding ray trajectories comprising up to 2 diffraction points are possible, also contribute to the interference patterns shown. This behavior changes for distances beyond a break point, corresponding, in the second region, to phase differences between rays being smaller than $\pi/2$.

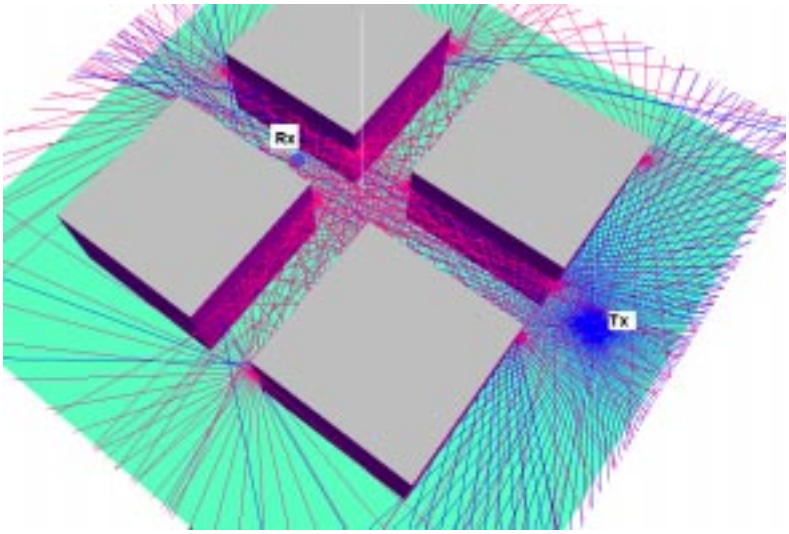

Figure 14 LOS case study: Pt=1W, f = 900Mhz, horizontal polarization, transmitter height = 15.6 m, receptor height = 1.7 m, 14 reflections and up to 2 diffractions considered

 ISSN 1516-7399

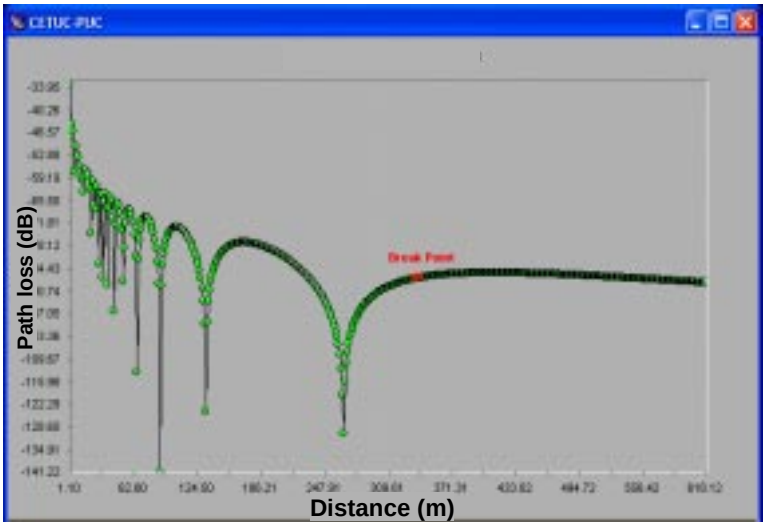

Figure 15 Predicted LOS path loss along crossing for the configuration in Figure 14

The power delay profile plot in Figure 17 shows the arrival times in (ns) of captured rays versus their amplitudes [dB] between the selected transmitter and receiver antennas, relatively to the arrival time of the LOS signal. One might also observe that, for received signals undergoing ray paths of negligible difference in length, corresponding relative power intensities depicted in Figure 17 may include more than one field contribution. This will not, however, significantly impact the calculation of more relevant channel parameters as the delay spread that can be derived from the power delay profile.

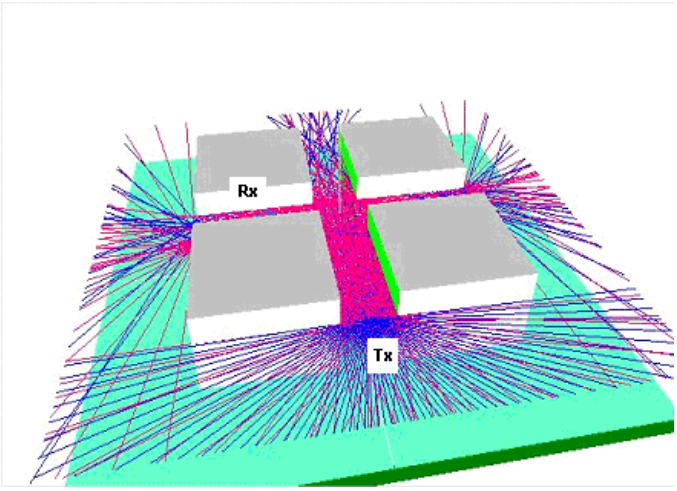

Figure 16 on LOS case study: Pt=1 W, f = 900 Mhz, horizontal polarization, transmitter height = 15.6 m, receptor height = 1.7 m, 14 reflections and up to 2 diffractions considered

 ISSN 1516-7399

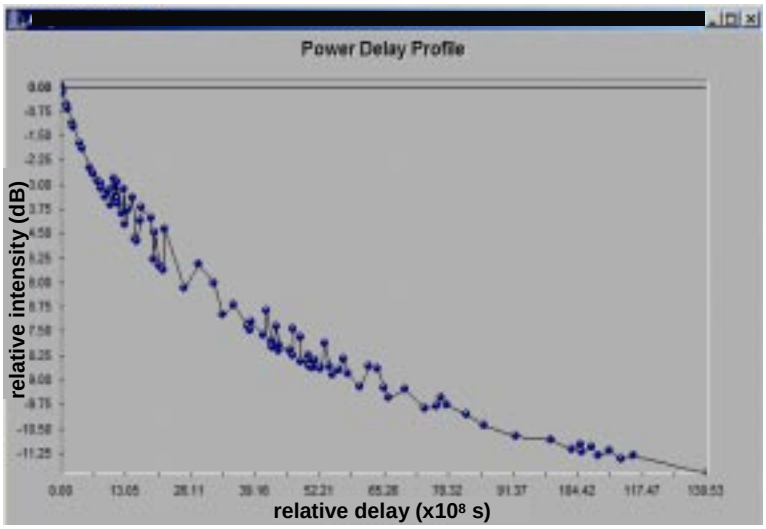

Figure 17 Power delay profile at the receiver end for the configuration in Figure 16

5. CONCLUSION

A ray tracing technique for coverage predictions in microcellular environments was summarized herein and a brief insight into underlying algorithms, otherwise detailed in [10], has been given. Presented results for basic environment cells illustrated the applicability of the technique for calculation of relevant radio channel parameters as power losses and delay profiles. Work in progress will encompass, besides the accommodation of more complex outdoor scenarios and/or indoor finer details served by diversified antenna systems, along with the implementation of more robust acceleration techniques, a comprehensive investigation of the role of higher-order scattering mechanisms in typical coverage predictions.

ACKNOWLEDGMENT

This work was supported by CNPq under Covenant PRONEX 664041/1996-S and by FINEP under Covenant FUNTTEL 0594/02.

REFERENCES

[1] R. G. Kouyoumjian and P. H. Pathak, A uniform geometrical theory of diffraction for an edge in a perfectly conducting surface, Proceedings of the IEEE, Vol. 62, 1974, pp. 1448-1461.

[2] G. D. Maliuzhinets, Excitation, reflection and emission of of surface waves from wedges of given face impedances, Soviet Phys. Doklady, Vol. 3, 1958, pp. 752-755.

[3] G. D. Maliuzhinets, Inversion formula for the Sommerfeld integral, Soviet Phys. Doklady, Vol. 3, 1958, pp. 52-56.

[4] T. B. A. Senior and J. L. Volakis, Approximate boundary conditions in electromagnetics, IEE Electromagnetic Waves Series 41, 1995, Ch. 4.

[5] M. Aïdi and J. Lavergnat, Comparison of Luebbers´ and Maliuzhinets´ wedge diffraction coefficients in urban channel modeling, in Progress in Electromagnetics Research, PIER 33, 2001, pp. 1-28.

[6] R. J. Luebbers, A heuristic UTD slope diffraction coefficient for rough lossy wedges, IEEE Trans. Antennas Propagat., Vol. AP-37, 1989, pp. 206-211.

[7] M. F. Cátedra and J. Pérez-Arriaga, Cell planning for wireless communications, Artech House – Mobile Communications Series, 1999.
[8] D. A. McNamara, C. W. I. Pistorius and J. A. G. Malherbe, Introduction to the uniform geometrical theory of diffraction, Artech House, 1990, pp. 185-188.
[9] M. E. C. Rodrigues, 3D ray tracing techniques for field calculation in indoor and outdoor environments, M. Sc. Thesis, EE Dept., PUC/Rio, 2000, in Portuguese.
[10] L.A.R. Ramirez, Técnica de Lançamento de Raios em Três Dimensões para a Previsão de Cobertura em Ambientes Micro-celulares, M. Sc. Thesis, EE Dept., PUC/Rio, 2002, in Portuguese.
[11] http://www.opengl.org
[12] D. J. Cichon, T. C. Becker and M. Döttling, Ray optical prediction of outdoor and indoor coverage in urban macro and micro-cells, in IEEE VTS 46th Vehicular Technology Conference, Atlanta GA, Vol. 1, 1996, pp. 41-45.
[13] B. E. Gschwendtner and F. M. Lanstorfer, 3-D Propagation modeling in microcell including terrain effects, in 6th IEEE Symposium on PIMRC, Vol. 2, 1995, pp 532-536.
[14] M. G. Sánchez, L. de Haro, A. G. Pino and M. Calvo, Exhaustive ray tracing algorithm for microcellular propagation prediction models, IEE Electronics Letters, vol. 32, No. 7, 1996, pp. 624-625.
[15] S. Y. Tan and H. S. Tan, Propagation model for microcellular communication applied to path loss measurements in Ottawa city streets, IEEE Transactions on Vehicular Technologies, Vol.44, No. 2, 1995, pp. 313-316..
[16] D. J. Cichon, T. Zwick and J. Lähteenmäki, Ray optical indoor modeling in multi-floored buildings: simulations and measurements, in IEEE Antennas and Propagation Society International Symposium Digest, vol. 1, 1995, pp. 522-525.
[17] G. Durgin, N. Patwari and T. S. Rappaport, Improved 3D ray launching method for wireless propagation prediction, IEE Electronics Letters, Vol. 33, No. 16, 1997, pp. 1412-1413.
[18] K. R. Schaubach, N. J. Davis and T. Rappaport, A ray tracing method for predicting path loss and delay spread in microcellular enviorements, IEEE 42nd Vehicular Technology Conference, Denver CO, vol. 2, 1992, pp. 932-935.
[19] W. Honcharenko, H. L. Bertoni, J. L. Dailing, J. Qian and H. D. Yee, Mechanics governing UHF propagation on single floors in modern office buildings, IEEE Transactions on Vehicular Technology, vol. 41, no. 4, 1992, pp. 496-504.

 ISSN 1516-7399